



A non-local approach based on the hypothesis of damage dissipation potential equivalence to the effect of stress gradient in fretting fatigue



Fei Shen, Weiping Hu*, Qingchun Meng

Institute of Solid Mechanics, School of Aeronautics Science and Engineering, Beihang University, Beijing 100191, China

ARTICLE INFO

Article history:

Received 13 November 2015
Received in revised form 20 April 2016
Accepted 27 April 2016
Available online 27 April 2016

Keywords:

Fretting fatigue
Stress gradient
Non-local approach
Continuum damage mechanics
Wear

ABSTRACT

A non-local approach based on continuum damage mechanics is proposed to take into account the stress gradient effect on fatigue crack initiation in fretting fatigue. The concept of subRVE (sub Representative Volume Element) is introduced as a smaller constituent unit of RVE (Representative Volume Element) and with the dimension of material average grain size for the purpose of considering the heterogeneous damage in the RVE. The fatigue damage in the subRVE is regarded as uniform, while the stress of subRVE is not uniform due to the effect of stress gradient. The fatigue damage evolution of each subRVE is derived by the hypothesis of damage dissipation potential equivalence with consideration of stress heterogeneity in the subRVE. Fretting fatigue is analyzed using this approach due to a zone of high stress gradient exists in the contact area. The predicted result from the proposed non-local model is better than that from local model by comparing with the experimental data. The interaction between wear and effect of stress gradient is also investigated.

© 2016 Elsevier Ltd. All rights reserved.

1. Introduction

Fretting fatigue is a process of damage accumulation which occurs when two bodies in contact experience small reciprocating motion and remote bulk fatigue stress. Due to the contact between the two bodies, fretting fatigue is characterized by severe stress gradient, which may be one order of magnitude larger than common notch fatigue configurations as reported by Fouvry et al. [1]. Significant effect of high stress gradient on the fretting fatigue life is observed in the experimental investigations [2,3].

The critical plane approaches were widely used to study the behavior of fretting fatigue [4–6]. In these approaches, the fretting fatigue life was predicted by using merely the local maximum value of fatigue damage parameter. Therefore, the effect of stress gradient was not considered. These approaches are also called local approaches. However, the existence of severe stress gradient in the contact zone can result in the failure of these local approaches. From the physical point of view, although the fatigue crack nucleates at the position with maximum stress firstly, the crack initiation involves a process of a crack growth to a small finite size, while the stress along the path is much less than the maximum stress under the presence of stress gradient. Therefore, the fatigue

damage is not only controlled by the stress–strain response of the maximum stressed point, but also the whole stress field in the zone covering the path. There are two other explanations for the phenomenon. One is suggested by Neuber [7] who suggested that the stress calculated by using the homogenous and isotropic material is not the true stress in the vicinity of the stress concentrator. Another is proposed by Miller [8] who believed that the spatial distribution of the stress field affects the capability of a crack to propagate.

In order to take the effect of stress gradient into account, some non-local approaches were then developed by averaging the multiaxial fatigue damage parameters over a specific volume or area. The dimension of the volume or area is a critical parameter in the non-local approaches. Three critical plane based parameters are evaluated by Naboulsi and Mall [9] to investigate the crack initiation behavior with the utilization of the volume process method. The effect of size of process volume on the averaged value of parameters was also studied. It was reported in [2] that a critical averaging dimension with the order of material grain size appears to give realistic estimates of fatigue life. Fouvry et al. [10] proposed a non-local approach, through which the multiaxial fatigue criterion was modified by a weight function to describe the gap between the predicted fatigue strength and the tested one. Besides, a non-local approach with stress-gradient-dependent critical dimension was also developed by Fouvry et al. [1], in which the critical dimension was expressed as a function of the hydrostatic

* Corresponding author at: Room D604, New Main Building, 37th Xueyuan Road, Beihang University, Beijing 100191, China.

E-mail address: huweiping@buaa.edu.cn (W. Hu).

Nomenclature

\mathbf{D}	tensor damage variable	R_v	tri-axiality function
D	scalar damage variable	A_{II}	amplitude of the octahedral shear stress
S	section area of the RVE	$\sigma_{H,mean}$	mean value of the hydrostatic stress
S_D	total area of micro-cracks or micro-voids in the RVE	$\sigma_{eq,max}$	maximum equivalent stress
S_R	effective area of resistance in the RVE	σ_{I0}	fatigue limit
$\bar{\sigma}$	effective stress	σ_u	ultimate tensile stress
σ	stress with damage	a, M_0, β, b_1, b_2	parameters of stress-based damage model
ε	strain	q	shear traction
ε_{ij}^e	elastic strain	ds	increment of local relative slip
ε_{ij}^p	plastic strain	θ	wear coefficient
E	initial elastic modulus	σ_{axial}	axial fatigue stress
ν	Poisson's ratio	F	normal force
α	backstress	Q	tangential force
σ_y	size of yield surface	R_s	axial stress ratio
\dot{p}	accumulated plastic strain rate	R_Q	tangential force ratio
λ	plastic multiplier	r	pad radius
C_k, γ_k	parameters of constitutive model	b	half width of specimen
ϕ	damage dissipation potential	d	thickness of specimen
Y	strain energy density release rate	μ	coefficient of friction
σ_H	hydrostatic stress	σ_R	reaction stress

pressure gradient. Although these averaging methods are able to provide predicted results consistent with the experimental data, numbers of empirical fatigue damage parameters are employed while their link with the physical explanation is not obvious.

Recently, the continuum damage mechanics (CDM) approach has been developed rapidly and has been introduced to the plain fatigue problems [11]. Generally, the fatigue life is predicted by using the local maximum stress in the dangerous RVE under the assumption that fatigue damage field in the RVE is uniform. However, significant discrepancies are observed between the results obtained by the local CDM approach and the experimental data for the case of high stress gradient. The non-local CDM method is then proposed. Marmi et al. [12] applied the Lemaitre–Chaboche fatigue mode [13] to predict the fatigue life of tensile samples with notches, in which the local approach and the non-local approach are compared. The generalized Papadopoulos formula [14] was applied to the equivalent stress used in the Lemaitre–Chaboche fatigue model and the critical distance was determined according to the distribution of the mean tri-axiality factor. Comparing to the experimental data, the non-local method gives reasonable estimate of the fatigue lives while the results predicted by the local approach are conservative.

CDM approaches have also been used to the fretting fatigue problem, including uncoupled CDM approach [15–17], coupled CDM approach [18,19], and coupled CDM approach in conjunction with the microstructure method [20]. For capturing the stress gradient effect, the similar strategy suggested in the literature [2] is also adopted in the uncoupled CDM approach. Stress-related variables in the damage evolution equation are averaged in the process zone having a dimension equal to the critical distance [15–17]. However, few non-local methods are investigated in the coupled CDM approach. The main reason may be that the fatigue damage is coupled in the constitutive model of material and therefore the stress redistribution is considered [18], which reduces the gap between the calculated stress and the real stress. Even though, the local method in the coupled CDM approach cannot give reasonable prediction of fretting fatigue life for some cases with high stress gradient.

Other aspect of the fretting fatigue is the phenomenon of wear. The effects of wear on the contact geometry, contact stress, subsurface stress and critical plane parameters are widely studied by

McColl et al. [21], Madge et al. [22,23] and Zhang et al. [24]. The results indicate that the predicted fretting fatigue life with considering the effect of wear is more reasonable, especially for the case of gross sliding. In the case of partial slip, the wear scar on the contact surface of the specimen is also observed in the fretting fatigue experiments [25]. From the investigation of the effect of wear conducted by Shen et al. [19,26], the wear is needed to take into account for the case of partial slip. Hence, the investigation of the interaction between wear and effect of stress gradient during the fretting damage becomes valuable.

In this study, a non-local method in the coupled CDM approach is proposed to investigate the fretting fatigue behavior under the partial slip condition. As we know, RVE is a basic concept of CDM, in which the damage is assumed to be uniform. However, this assumption is unreasonable when obvious stress gradient exists in material. For the purpose of considering the heterogeneous damage caused by the stress gradient effect, the concept of subRVE is introduced as a smaller constituent unit of RVE and with the dimension of material average grain size. The fatigue damage in the subRVE is regarded as uniform, while the stress of subRVE is not uniform due to the effect of stress gradient. The damage evolution of each subRVE is derived based on the hypothesis of damage dissipation potential equivalence. The damage coupled Chaboche plasticity model is used to calculate the stress–strain response of the fretting contact and the effect of wear is also considered. The predicted results by the non-local approach are compared to the experimental data and the results by the local approach, and the interaction between wear and effect of stress gradient is also investigated.

2. Models

In this section, the damage variable is defined in the framework of CDM firstly, in which isotropic damage is assumed and the damage variable is a scalar D . Then, the damage coupled Chaboche plasticity model is introduced to calculate the stress–strain response under fretting fatigue loadings. A non-local fatigue damage model based on the hypothesis of damage dissipation potential equivalence (DDPE) is proposed to accumulate the fatigue damage of subRVEs. In order to take the effect of wear into account, the

energy wear model is implemented to change the contact geometry progressively, which is presented in the end of this section.

2.1. Damage variable

According to the definition given by Lemaitre and Rodrigue [11], material damage in its mechanical sense is the creation and growth of micro-voids or micro-cracks which are discontinuities in a medium considered as continuous at a larger scale. Further, Murakami [27] depicted that the microscopic mechanism of material damage consists of four mechanisms, cleavage, growth and coalescence of micro-voids, glide plane decohesion, and void growth due to grain-boundary diffusion. For the case of the formation of fatigue crack, the dislocation pileup, irreversible slip and the consequential formation of persistent slip bands play key roles in the mesoscopic perspective. Thus, McDowell et al. [28,29] directly adopted microstructure methods to establish the model of fatigue crack formation by calculating the local accumulated micro-plastic strain and simulating the formation of the persistent slip bands. From the physical point of view, the accumulated slip will eventually induce the separation of material in the form of micro-voids or micro-cracks. Therefore in the framework of CDM, the accumulated slip which plays key roles in the formation of fatigue crack is actually included in the damage model. Researchers have proposed some damage models for the failure analysis of ductile, brittle, fatigue, creep and creep-fatigue damage problems [11]. In engineering, the mechanics of continuous media can be described by a RVE in which all mechanical properties are represented by homogenized variables, as shown in Fig. 1 [15]. It is worth noting that the RVE is actually a smallest material element in the continuum mechanics computation or analysis, the dimension of which depends on the microstructure of materials, such as for metals, 0.1 mm³ is a common value used in analysis. In the framework of continuum damage mechanics, damage of materials is assumed to be uniform in a RVE. Then, the damage variable **D**, used to describe the damage value of RVE, associated with the direction of the normal vector \vec{n} is defined as

$$D_n = \frac{S_D}{S} \quad (1)$$

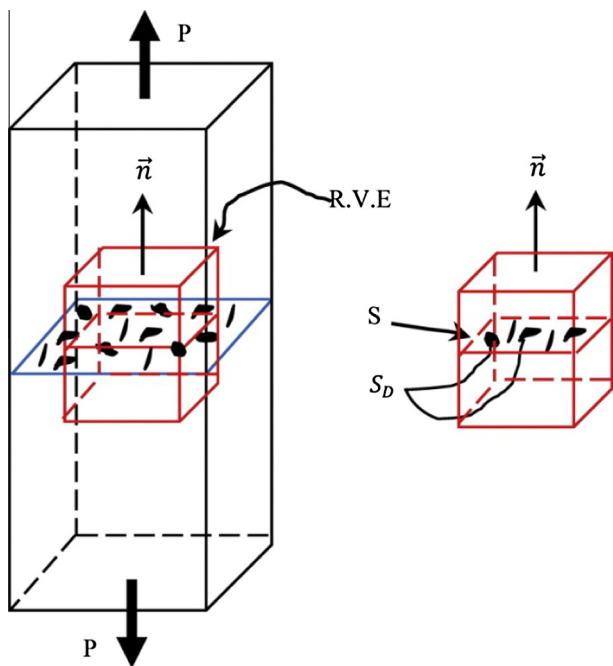


Fig. 1. Representative Volume Element (RVE).

where S is the area of a section of the RVE identified by its normal vector and S_D is the total area of micro-cracks or micro-voids, which constitute the damage. In this work, isotropic damage is assumed, in which case the damage tensor **D** is reduced to a scalar variable D

$$D = \frac{S - S_R}{S} \quad (2)$$

where S_R represents the effective area of resistance, $S_R = S - S_D = (1 - D)S$. The effective stress $\tilde{\sigma}$ is introduced to describe stress over the section, which effectively resists the forces

$$\tilde{\sigma} = \frac{P}{S_R} = \frac{P}{(1 - D)S} = \frac{\sigma}{1 - D} \quad (3)$$

where P is the total load acting on the section with the area of S . The variable σ is the stress for the damaged material. Different definitions of damage can be found in the works of Voyiadjis and Kattan [30,31] and the same equation as Eq. (3) is deduced based on the hypothesis of strain equivalence.

The definition of damage variable is suitable for the condition of uniform stress in the whole RVE. While, due to the presence of high stress gradient, the stress distribution in a RVE can be regarded to be neither uniform nor approximately uniform. Consequently, the damage in RVE is not uniform or approximately uniform. Thus, the direct use of continuum damage mechanics based approach will induce unreasonable predicted result. For the purpose of considering the heterogeneity of damage in RVE, a similar definition of damage variable is defined on the scale of a smaller portion of RVE, namely subRVE. In this study subRVE is assumed to be a constituent unit of RVE and it has the dimension of material average grain size which is, such as, 10 μm for Ti-6Al-4V and 20–50 μm for aluminum alloy. The relevant fatigue damage model will be presented in Section 2.3.2.

2.2. Damage coupled Chaboche plasticity model

In the fretting fatigue, the elasto-plastic constitutive model is more appropriate to use as one calculates the stress and strain in the contact zone where plastic deformation may occur due to the stress concentration. The Chaboche plasticity model [32] is adopted in this study due to its simplicity and ease to use. With consideration of the fatigue damage, the damage variable is coupled into the Chaboche plasticity model by using the effective stress instead of the stress used in the elasticity law and in the Mises yield criterion, which is based on the hypothesis of strain equivalence. The basic equations of damage coupled elasto-plastic constitutive model are listed below [11]:

- The decomposition of total strain for small strains is expressed by

$$\varepsilon_{ij} = \varepsilon_{ij}^e + \varepsilon_{ij}^p \quad (4)$$

where ε_{ij}^e and ε_{ij}^p are the elastic strain and plastic strain, respectively.

- The elasticity law with damage is expressed by

$$\varepsilon_{ij}^e = \frac{1 + \nu}{E} \left(\frac{\sigma_{ij}}{1 - D} \right) - \frac{\nu}{E} \left(\frac{\sigma_{kk} \delta_{ij}}{1 - D} \right) \quad (5)$$

where E and ν are the elastic modulus and Poisson's ratio of the undamaged material, respectively. The variable σ_{ij} is the Cauchy stress of the damaged material.

- The yield function and plastic flow with damage is expressed by

$$F = \left(\frac{\sigma_{ij}}{1 - D} - \alpha_{ij} \right)_{eq} - \sigma_y \quad (6)$$

$$\dot{\varepsilon}_{ij}^p = \dot{\lambda} \frac{\partial F}{\partial \sigma_{ij}} = \frac{3}{2} \frac{\dot{\lambda}}{1 - D} \left(\frac{\sigma_{ij}}{1 - D} - \alpha_{ij} \right)_{dev} \quad (7)$$

$$\dot{p} = \sqrt{\frac{2}{3} \dot{\epsilon}_{ij}^p \dot{\epsilon}_{ij}^p} = \frac{\dot{\lambda}}{1-D} \quad (8)$$

The subscript ‘dev’ and ‘eq’ represent the deviatoric component of the stress and the von Mises equivalent stress, respectively. The term α_{ij} is the deviatoric component of the back stress, $\dot{\lambda}$ is the plastic multiplier and \dot{p} is the accumulated plastic strain rate. The term σ_y represents the size of the yield surface which is assumed to remain unchanged in this study.

- The hardening law with damage is expressed by

$$\alpha_{ij} = \sum_{k=1}^{N_{bs}} \alpha_{ij}^{(k)} \quad (9)$$

$$\dot{\alpha}_{ij}^{(k)} = (1-D) \left(\frac{2}{3} C_k \dot{\epsilon}_{ij}^p - \gamma_k \alpha_{ij}^{(k)} \dot{p} \right) \quad (10)$$

where N_{bs} is the number of the back stress components. Parameters C_k and γ_k are material constants determined from experimental tests.

It should be noted that the reason why we still adopt the anisotropic continuum plasticity model instead of crystal plasticity approaches used in Refs. [28,33–35] is based on two points. The first is that the proposed approach in this study may be regarded as an improved continuum damage mechanics based approach, that is to say, it is still in the framework of continuum damage mechanics although the subRVE has a dimension of grain size. The second is that the coupled damage model based on the continuum damage mechanics is much less time-consuming than microstructure based approach, and it can provide a reasonable life prediction as well.

2.3. Fatigue damage models

Two fatigue damage models are presented in the following two subsections, respectively. A common used fatigue damage model for high cycle fatigue is introduced briefly, in which the effect of stress gradient is neglected. Then, a non-local fatigue damage model is proposed on the basis of the former fatigue damage model.

2.3.1. Local fatigue damage model

For fatigue problem, the damage variable of RVE is accumulated with increasing fatigue loading cycles. The initiation of macro-crack takes place once the damage variable reaches a critical value.

Fatigue damage is related to the irreversible energy dissipation of the RVE during fatigue loadings. The form of the damage dissipation potential ϕ is written as proposed by Lemaitre [36] as:

$$\phi = \phi(Y, \dot{Y}; T, D, \sigma) \quad (11)$$

where parameter T represents the temperature and variable Y is the strain energy density release rate derived from the thermodynamic potential, expressed by

$$Y = \frac{\sigma_{eq}^2}{2E(1-D)^2} R_v \quad (12)$$

where σ_{eq} is the Von Mises stress and R_v is the tri-axiality function, written as:

$$R_v = \frac{2}{3}(1+\nu) + 3(1-2\nu)(\sigma_H/\sigma_{eq})^2 \quad (13)$$

where σ_H is the hydrostatic stress. The damage evolution law is derived from Eq. (11) by differentiating ϕ with respect to Y , given as:

$$\dot{D} = \frac{\partial \phi}{\partial Y} \quad (14)$$

A detailed research was carried out by Xiao et al. [37] to deduce a continuum damage mechanics model for uniaxial fatigue loadings from Eq. (14), in which the Lemaitre and Chaboche (LC) fatigue damage model [13] was also obtained. For fretting fatigue, the stress status in the contact zone is multiaxial and therefore the 3D form of LC fatigue damage model [12,18,38] is suitable to describe the damage evolution, which is expressed as:

$$\frac{dD}{dN} = [1 - (1-D)^{\beta+1}]^\eta \left[\frac{A_{II}}{M_0(1-3b_2\sigma_{H,mean})(1-D)} \right]^\beta \quad (15)$$

where A_{II} is the amplitude of octahedral shear stress, expressed by

$$A_{II} = \frac{1}{2} \left[\frac{3}{2} (s_{ij,max} - s_{ij,min})(s_{ij,max} + s_{ij,min}) \right]^{1/2} \quad (16)$$

where $s_{ij,max}$ and $s_{ij,min}$ are the maximum and minimum values of the deviatoric stress during one loading cycle. $\sigma_{H,mean}$ is the mean value of hydrostatic stress

$$\sigma_{H,mean} = \frac{1}{6} (\sigma_{kk,max} + \sigma_{kk,min}) \quad (17)$$

Parameter η is defined with the Sines fatigue limit criterion [39] as

$$\eta = 1 - a \left\langle \frac{A_{II} - A_{II}^*}{\sigma_u - \sigma_{eq,max}} \right\rangle \quad (18)$$

$$A_{II}^* = \sigma_{I0}(1 - 3b_1\sigma_{H,mean}) \quad (19)$$

where $\sigma_{eq,max}$ is the maximum equivalent stress over a loading cycle. σ_{I0} is the fatigue limit at the fully reversed loading condition and σ_u is the ultimate tensile stress. Five parameters, a , M_0 , β , b_1 , b_2 , are determined by using plain fatigue tests of standard specimens. The ultimate tensile stress σ_u is obtained from monotonic tensile stress strain curve. Parameters σ_{I0} and b_1 are obtained from the fatigue limit data at different mean stress. Parameters β and $aM_0^{-\beta}$ can be get using the least square method fitting S–N curve of stress-controlled fatigue test of smooth specimen at fully reversed loading condition. Further, parameter b_2 can be determined fitting S–N curves of fatigue tests at different mean stresses. Finally, parameter a is identified using the numerical method introduced by Zhang et al. [18].

It is worth noting that LC fatigue damage model presented above was built on the assumption of uniform stress field in the whole RVE. The fatigue damage is also uniform in the RVE in such condition. In the actual application to the fatigue life prediction of engineering components, the fatigue damage accumulation is calculated on each finite element by substituting the local stresses into the LC fatigue damage model. Therefore, two conditions need to be concerned when applying this method. One is that the dimension of finite element should be almost equal to that of RVE, and another is that the stress of finite element should be approximately uniform.

The above damage model is stress based which is for the case of elastic damage. It is noticed that we will use this model for the damage analysis of subRVE. That is based on two facts. Firstly, at the beginning, the plastic strain is non-existence for all nine experiments because the loadings are not high enough. Secondly, the plastic strain may occur due to the change of contact geometry induced by wear. However, the contact geometry changes little in the studied cases. The magnitude of the plastic strain is also very small. Consequently, the plastic damage is negligible compared to the elastic damage. Therefore, we do not consider plastic damage in this study. However, we adopt the damage coupled elastic–plastic model to conduct the stress analysis. Because although the value of plastic strain is small and the corresponding plastic damage is neglected, the deviation between the results of stress calcu-

lated by elastic–plastic constitute model and elastic constitute model is needed to be considered.

2.3.2. Non-local fatigue damage model based on DDPE

Under the circumstance of severe stress concentration or high stress gradient, the stress field in the range of dimension of RVE (it is usually 0.1 mm^3 for metals) is no more uniform and the damage dissipation potential cannot be expressed as Eq. (11). It is reported by Marmi et al. [12] that the deviations on the predicted fatigue lives by using the LC fatigue damage model directly with the experimental data are significant for notched specimens with material Ti–6Al–4V. Besides, the fatigue damage and initiated fatigue crack is localized in a very small area of the experimental specimen, such as at the notch tip. The length of the initial macro-crack is considered as with the same magnitude of the average grain size although it may be dependent on the accuracy of measure method, which is much smaller than the size of RVE. Therefore, the assumption of uniform fatigue damage in the whole RVE is unreasonable under the condition of high stress gradient.

In this subsection, a non-local fatigue damage model is proposed to deal with the effect of stress gradient. Firstly, due to the non-uniform damage in the RVE, we divide the whole RVE into many subRVEs, and the subRVE is assumed to be the minimum material element when conducting damage calculation. Hence, the damage of a subRVE is regarded as uniform although the stress of each subRVE remains to be heterogeneous due to the existence of stress gradient. The dimension of subRVEs is associated with the average grain size of material, which then have the physical meaning because generally the fatigue crack initiation is defined when a crack with the length of grain size appears in material. The dimension of subRVE is taken as $20 \mu\text{m}$ in this study. From the point of physical point view, RVE is a material element whose mechanical properties are homogenized over all grains contained in the RVE, while subRVE with the dimension of grain is a smaller constituent material element of RVE, whose mechanical properties are allowed to be different from each other. One may imagine subRVE as grain but it is actually not real grain in this study, because we just assume the scale of subRVE being the same with grain while do not relate to the real shape and distribution of grain, not as some microstructure-based method adopted by researchers. Once the fatigue damage of the most dangerous subRVE reaches a critical value, the specific subRVE breaks thoroughly, meaning the macro-crack initiates at the position of that subRVE. It should be noted that it is difficult to accurately define a crack length corresponding to the crack initiation. According to the traditional definition, it is defined when the appearance of crack is detectable by the usual control means. However, the length of crack is ambiguous. Researchers gave different length definitions according to the particular cases [40–42], among which the grain size is the one [34,35]. In this study, we assume that the failure of subRVE with the dimension of averaging grain size indicates the crack initiation. The failure of subRVE is defined when the damage value of subRVE reaches a critical value. It should be noted that this failure criterion of subRVE is not proposed directly based on the experimental observation but from a phenomenological view. On the one hand, the damage value of subRVE just represents the deterioration of mechanical properties of subRVE not definitely corresponding to the real micro-cracks in the subRVE. On the other hand, because we assumed that subRVE is the minimum material element in damage analysis, thus it is natural to define the failure of subRVE when its damage value reaches the critical value.

Secondly, it is critical to calculate the evolution of fatigue damage for each subRVE within which stress gradient exists. A hypothesis of damage dissipation potential equivalence is applied to derive the damage evolution equation of each subRVE. Based on this hypothesis the homogenized damage of a subRVE is expressed

by the dissipation potential and energy density release rate of the whole subRVE. The derivation is presented as follows.

According to Eq. (14), the rate of local damage dissipation potential ϕ can be written as:

$$d\phi = \frac{dD}{dt} dY \quad (20)$$

Integrating Eq. (20) over one cycle to obtain the increment of ϕ during the cycle, and assuming the increment of D to be independent on the integrating calculation because its value is very small during one loading cycle, then gives

$$\Delta\phi = \int_{1 \text{ cycle}} d\phi dt = \int_{1 \text{ cycle}} dD dY = \Delta D \int_{1 \text{ cycle}} dY = \Delta D \Delta Y \quad (21)$$

The total increment of ϕ in subRVE is calculated by integrating Eq. (21) over the volume of subRVE, which is written as

$$\int_{\text{subRVE}} \Delta\phi dV = \int_{\text{subRVE}} \Delta D \Delta Y dV \quad (22)$$

Two variables are then introduced as D_{subRVE} and Y_{subRVE} , which represent the homogenized fatigue damage and the total damage strain energy density release rate for subRVE. According to Eqs. (21) and (22), a critical equation is derived as

$$\Delta D_{\text{subRVE}} \Delta Y_{\text{subRVE}} = \int_{\text{subRVE}} \Delta D \Delta Y dV \quad (23)$$

where ΔY_{subRVE} can be written as

$$\Delta Y_{\text{subRVE}} = \int_{\text{subRVE}} \Delta Y dV \quad (24)$$

Therefore, the increment of homogenized fatigue damage for subRVE is calculated as

$$\Delta D_{\text{subRVE}} = \frac{\int_{\text{subRVE}} \Delta D \Delta Y dV}{\int_{\text{subRVE}} \Delta Y dV} \quad (25)$$

According to the equations derived above, the increment of damage of each subRVE can be calculated using the local LC fatigue model. In the actual calculation, the integral calculation in Eq. (25) is applied in each subRVE comprising several elements. Therefore, Eq. (25) can be written as

$$\Delta D_{\text{subRVE}} = \frac{\sum_{k=1}^{N_{pt}} (\Delta D_k \Delta Y_k)}{\sum_{k=1}^{N_{pt}} \Delta Y_k} \quad (26)$$

where ΔD_k and ΔY_k represent the increments of local fatigue damage and damage strain energy density release rate at k th integration point in subRVE, respectively. N_{pt} is the total number of integration points in each subRVE.

It is worth noticing that the fatigue damage of each subRVE calculated by using the equivalence of damage dissipation potential, strictly speaking, is not the average damage of subRVE. Actually, in a sense, it is a homogenization of damage field within a subRVE based on the hypothesis of damage dissipation potential equivalence.

2.4. Energy wear model

The energy wear model considers the interfacial shear work as the significant wear parameter controlling wear volume calculation.

$$V = \theta \sum W_{\text{shear}} \quad (27)$$

where θ is the wear coefficient and $\sum W_{\text{shear}}$ is the accumulate shear energy. The shear energy is the frictional dissipation energy on the contact surface, defined by the product of frictional force and the relative slip displacement. For 2D fretting model, at time t and

position x along the contact surface, the local wear depth can be expressed as follows [24]

$$h(x, t) = \theta \int_{t=0}^t q(x, t) ds(x, t) \quad (28)$$

where $q(x, t)$ is the local shear traction and $ds(x, t)$ is the increment of local relative slip. Parameter θ is a critical constant determined through the wear experiment.

3. Experiments and finite element model

The fretting fatigue experiments carried out by Hojjati-Talemi et al. [17] are used to validate the proposed approach. The tested material is aluminum 2024-T3, a tempered aerospace aluminum with good fatigue properties. The method of the parameters identification for the above models is presented in the literature [19] and the parameters for 2024-T3 are determined by using experimental data from the literature [17,43,44], which are listed in Table 1.

It should be noted that the wear coefficient is one of parameters should be determined by the wear experiment with the same contact conditions. However, the wear properties of aluminum alloy contact are unavailable in the fretting fatigue experiments [17] analyzed in this paper. As reported by Magaziner et al. [45], the wear coefficient was influenced by many factors, such as material hardness, relative slip amplitude and contact load. It is difficult to obtain the wear data under the same contact conditions in [17] from the published literature. To our knowledge at present, majority of wear experiments involving aluminum alloys can be classified to three catalogs. The first type is for aluminum alloys contacting with other materials; the second type is for aluminum alloys with different coating films and the third type is for aluminum metal matrix composites. Therefore, approximately, we use the fretting wear experiments [46] involving glass-fiber-reinforced polypropylene composite on aluminum alloy to determine the wear coefficient of 2024-T3, as shown in Fig. 2. This wear coefficient is treated as an estimated value for the fretting fatigue experiments in this research. The scope of the fitting curve is $1 \times 10^{-5} \text{ mm}^3/\text{J}$ and the parameter θ in Eq. (28) is then set as $1 \times 10^{-8} \text{ MPa}^{-1}$. Because of the inaccuracy of the wear coefficient, it is needed to evaluate the sensitivity of the coefficient on the predicted results. The effect of wear coefficient will be presented in Section 5.5.

Considering that the plane strain assumption can be applied for this study, the 2D schematic view of the fretting fatigue experiments is shown in Fig. 3 [17]. The axial cyclic load σ_{axial} was applied on the dog-bone specimen. The constant normal forces F were applied on two pads by two single servo-hydraulic actuators. The load cells were used to keep the contact normal forces constant in experiments. The tangential force Q between the specimen and the pads was generated by means of leaf springs. The compliance of the leaf springs and the deformation of the specimen generate the tangential force, which is proportional to the axial cyclic load. The fretting fatigue experiments were performed under the conditions such as axial stress ratio $R_s = 0.1$, tangential load ratio

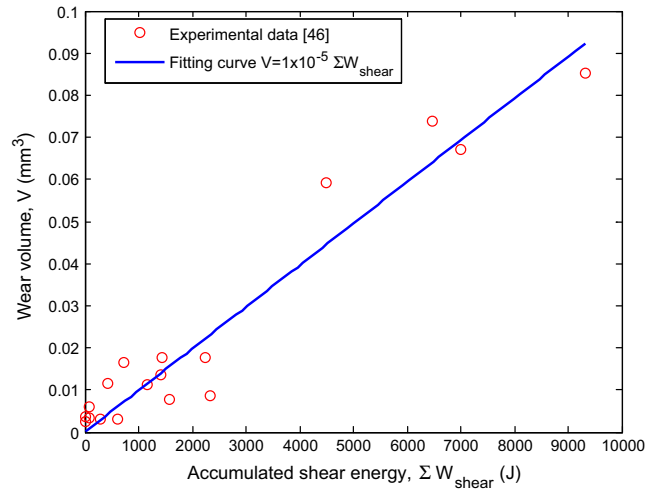


Fig. 2. Variation of wear volume with accumulated shear energy [46].

$R_Q = -1$ and test frequency $f = 10$ Hz. The additional parameters for fretting fatigue experiments were kept constant for all the experiments: $F = 543$ N; pad radius $r = 50$ mm.

Based on the symmetric configuration, one half of the fretting contact is modeled by using ABAQUS, as shown in Fig. 4. The coordinate system is also shown in Fig. 4, in which the origin of the coordinate plane is at the midpoint of the contact zone along the surface of the specimen. The half width of specimen (along y axis) is $b = 5$ mm. The thickness of specimen (along z axis) is $d = 4$ mm while this dimension is not involved in numerical simulation because the plane strain assumption is made to approximately simulate the real three dimensional contact problem. This assumption is acceptable because, in the study, two pads pressed on the two sides of the specimen in the width direction, meanwhile, the axial fatigue stress is positive on the one end of the specimen. The combined effects of these forces make the deformation of the specimen along the width direction unobvious. This assumption was also adopted by other researchers [23,24]. Besides, the analytical semi contact width is $a = 0.462$ mm. The contact between the fretting pad and the specimen is defined using the master-slave algorithm for contact between surfaces. Coulomb friction is employed based on the Lagrange multiplier contact algorithm to ensure the exact stick condition when the shear stress is less than the critical shear value. A constant coefficient of friction COF of $\mu = 0.65$ is considered throughout the analyses [17,44]. The element length and width in the contact zone are both $10 \mu\text{m}$. A mesh convergence study is conducted to verify the appropriateness of the current mesh size in the contact region between the pad and the specimen. Fig. 5(a) and (b) shows a good correlation between FE results and theoretical solutions for the contact pressure and shear traction along the contact surface.

The constant normal force F is applied to the top face of the pad by using the Multi-Point Constraint (MPC) method. The axial cyclic stress σ_{axial} is loaded at the right side of the specimen, as illustrated

Table 1
Material parameters for 2024-T3.

E (MPa)	ν	σ_y (MPa)	C_1	γ_1	C_2	γ_2	σ_u (MPa)
74,100	0.33	383	9410	387.2	5530.2	38.1	506
σ_{10} (MPa)	β	$aM_0^{-\beta}$	b_1	b_2	a		
124	2.1479	5.925e-11	6.744e-4	1e-5	0.75		

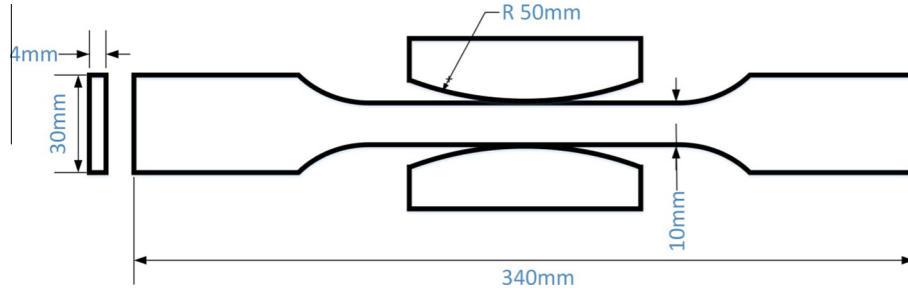


Fig. 3. 2D schematic view of the fretting fatigue experiments.

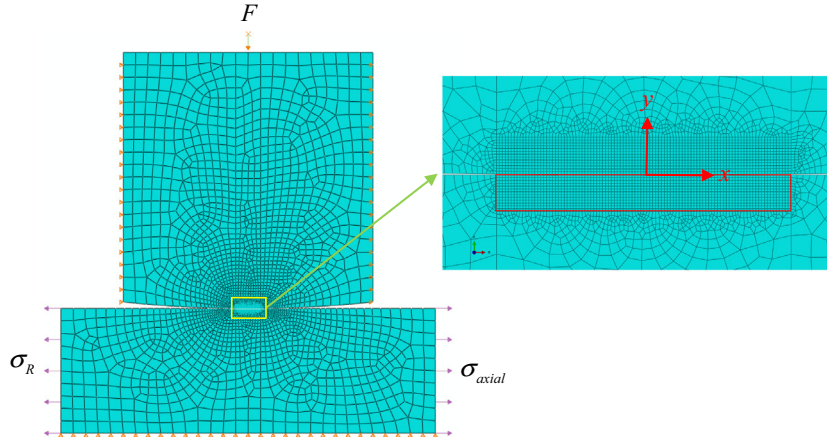


Fig. 4. Finite element model of fretting contact.

in Fig. 4. The modeling method proposed by Hojjati-Talemi and Wahab [15] is used to apply the tangential force Q . Both sides of cylindrical pad are restricted to move just in the vertical direction. The tangential force, which is in phase with the axial cyclic stress, is defined by subtracting the reaction stress applied on the left side of specimen from the axial cyclic stress.

$$\sigma_R = \sigma_{axial} - \frac{Q}{bd} \quad (29)$$

where σ_R is the reaction stress at the left side of the specimen. Based on two loading ratios, R_s and R_Q , the loading history of σ_R can be calculated as shown in Fig. 6.

4. Numerical algorithm

In this section, the numerical algorithm is presented to simulate the behavior of fretting fatigue crack initiation. Three models mentioned above are implemented by utilization of the subroutines UMAT and UMESHMOTION in ABAQUS.

The subsurface stress, contact stress and relative slip are calculated by using the damage coupled Chaboche plasticity model. During each fatigue loading cycle, the wear simulation is carried out after each time increment forming the new the contact geometry. The fatigue damage accumulation for each subRVE is carried out at the end of each loading cycle. Firstly, according to the history of stress field during this loading cycle in each subRVE, the increment of the local fatigue damage, ΔD_k , can be calculated by the local LC fatigue model, and the increment of the damage strain energy density release rate, ΔY_k , can also be obtained by using the stress history during one cycle. The fatigue damage increment of subRVE, ΔD_{subRVE} , can then be calculated using Eq. (26). The total fatigue damage of subRVE is updated, which is followed by the

simulation of next fatigue loading cycle. This procedure continues until the fatigue damage of any subRVE reaches the critical value.

Due to the fretting contact, stress concentration mainly locates at the contact surface of the specimen, especially at the contact edge. Thus, the effect of stress gradient in the central contact zone of the specimen, marked by red rectangle in Fig. 4, is needed to be considered. The non-local fatigue damage model proposed in this study is used in this zone, while the local fatigue damage model is still suitable to predict the evolution of damage in the other zone of the specimen. As depicted in Fig. 7(a), the central contact zone is divided by a group of subRVEs. In this study, the dimension of subRVE is determined to be 20 μm according to the investigations on the average grain size of aluminum 2024-T3 in [47,48]. A schematic view of one subRVE is illustrated in Fig. 7(b), which is constituted by four elements. It should be noted that there are two patterns of arrangement of the subRVEs for this studied case. While the difference between results from these two patterns is negligible. Therefore, we just present one of them here.

It is worthy to notice that the grid of subRVE in Fig. 7(a) does not represent the actual crystallographic structure. Compared to the CDM approach, a more direct and sophisticated one is micro-structure approach [30–33] which simulates the fatigue crack formation at the scale of material grain. The real shapes and pattern of crystals in material are modeling by finite element method and the stress and plastic strain are calculated by crystal plasticity model. The behavior of fatigue crack initiation is studied by certain mesoscopic fatigue indicator parameters. However, the micro-structure approach is beyond the scope of this study.

Since it is computationally expensive to simulate each loading cycle, the jump-in-cycles procedure [11] is adopted in the numerical implementation, which assumes that the stress and damage remain unchanged for a finite period of ΔN cycles constituting a block. Then the damage evolution can be interpreted as piecewise

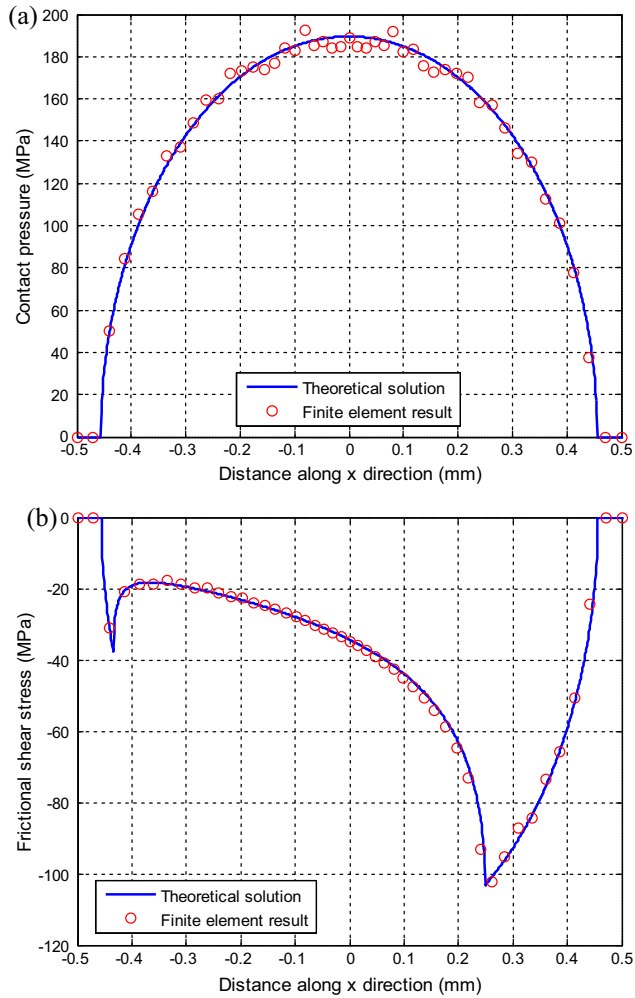


Fig. 5. Comparisons of finite element results of (a) contact pressure and (b) shear traction along the contact surface with the theoretical solutions for $\sigma_{axial} = 100$ MPa, $Q_{max} = 155.165$ N.

linear with respect to the number of cycles. It is necessary to note that the value of ΔN is determined to obtain a convergent fretting fatigue life. The detailed steps of the numerical implementation are listed as follows:

- (1) The initial damage for each integration point of each element is assumed to be zero.
- (2) The damage coupled Chaboche constitutive equations, Eqs. (4)–(10), are solved to obtain the stress–strain response for the current block of cycles, including the contact stress and relative slip between the pad and the specimen.
- (3) The wear simulation is carried out after each time increment. The increment of wear depth for each node along the contact surface is calculated and implemented by moving the node against the local normal direction at the end of each time increment. The contact geometry changes gradually, which affects the stress–strain response. During each block of cycles, three steps that are used to implement the energy wear model are listed below:

- (a) For a contact node, the increment of local wear depth at the k th time increment for a block is given as

$$\Delta h = \phi \Delta N q_k \Delta s_k \quad (30)$$

where q_k and Δs_k are shear traction and incremental slip for the k th time increment, respectively. The increment of

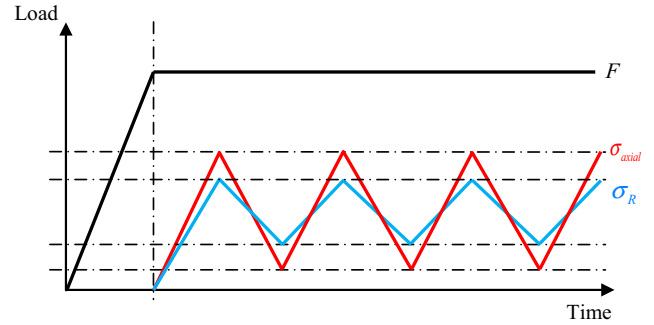


Fig. 6. Schematic view of fretting loading history.

local wear depth, Δh , is implemented by moving the surface nodes against the local normal direction at the end of each time increment.

- (b) The material variables are re-mapped to the new position by solving the advection equations using a second order numerical method termed the Lax–Wendroff method [49].
- (c) Repeat steps (a) and (b) until the number of time increment k reaches the maximum number of time increment within one fretting cycle, K_{max} . For the purpose of determining an appropriate value of K_{max} . We calculated with two values, 100 and 40, respectively. The results have negligible difference from each other with. Therefore, in order to save the computation costs, we take $K_{max} = 40$ in this study.
- (4) After each block of cycles, the following three steps are used to update the damage value of subRVE and the number of cycles. These steps are listed below:
 - (a) Two variables, ΔD_k and ΔY_k , at the k th integration point in subRVE can be obtained by using the history of stress during one cycle. Then, the fatigue damage increment of subRVE is calculated by

$$\Delta D_{subRVE,j}^i = \frac{\sum_{k=1}^{N_{pt}} (\Delta D_k \Delta Y_k)}{\sum_{k=1}^{N_{pt}} \Delta Y_k} \quad (31)$$

where i represents the current block of cycles and j is the number of subRVE. N_{pt} represents the total number of the integration points in each subRVE.

- (b) The damage value and the number of cycles for the j th subRVE are updated at the end of the current block of cycles

$$D_{subRVE,j}^{i+1} = D_{subRVE,j}^i + \Delta D_{subRVE,j}^i \Delta N \quad (32)$$

$$N^{i+1} = N^i + \Delta N \quad (33)$$

It is an explicit method and the accuracy of the predicted results is relevant with the value of ΔN . A central or backward difference method would be superior. However, the results obtained by these three methods are almost identical when the value of ΔN meets the relation of $\Delta N/N_i \approx 0.01 \sim 0.02$ [18,19]. In this study, the appropriate value of ΔN is chosen according to this relation to obtain convergent result. Besides, after an appropriate value of ΔN is determined, a constant value of ΔN will be used in the life prediction of one load condition. However, different values of ΔN may be used for the cases under different load conditions.

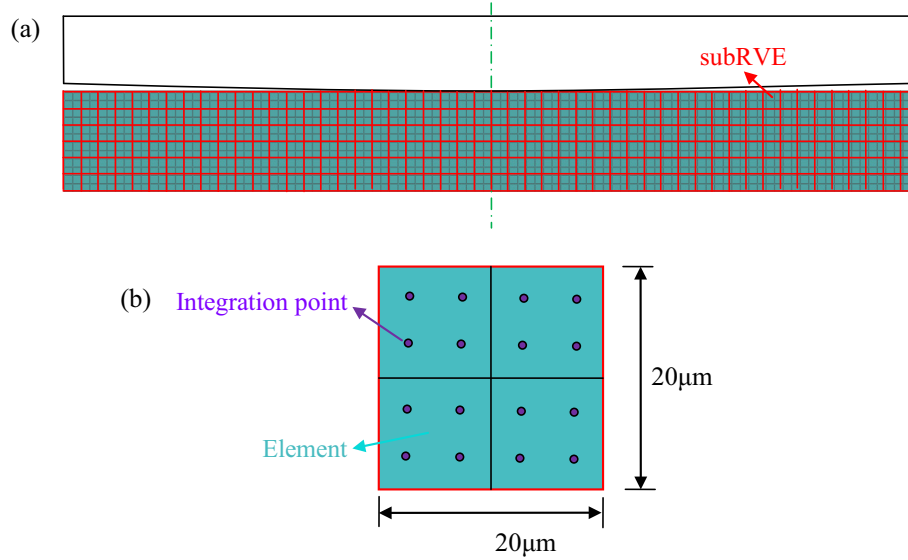


Fig. 7. Schematic view of (a) the group of subRVE in the contact zone of the specimen, (b) one subRVE.

(c) The fatigue damage value at each integration point in the j th subRVE is set to the value calculated by Eq. (32).

(5) The algorithm repeats steps (2)–(4) for each block of cycles until the accumulated damage of any integration point reaches the critical value D_c . The number of cycles at this stage is the fretting fatigue crack initiation life. In this study, the critical value is set to 1.

5. Results and discussion

5.1. Computational result and analysis

Nine fretting fatigue experiments are conducted in the literature [17], the test conditions of which are listed in Table 2. All the tests fall into the partial slip regime due to that the loading conditions meet the equation $Q_{max} < \mu F$. The fatigue crack initiation behaviors of the tests are simulated by the proposed non-local CDM approach with wear. The predicted fretting fatigue initiation lives are listed in the last column of Table 2, which agree well with the experimental fatigue crack initiation lives $N_{exp,i}$.

It should be noted that the Ref. [17] did not provide the experimental crack initiation life. The experimental data in Ref. [17] is the total fatigue life, including the fatigue crack initiation life and the crack propagation life. They compared their predicted total life with the experimental data while did not compare these two parts separately. Finally, they estimated the percentage of fretting fatigue crack initiation and propagation lifetime for each case on the

Table 2
Test conditions of fretting fatigue experiments [17].

Test no.	σ_{axial} (MPa)	Q_{max} (N)	$N_{exp,f}$	$N_{exp,i}$	$N_{pred,i}$
FF1	100	155.165	1,407,257	809,650	650,000
FF2	115	186.25	1,105,245	681,320	464,000
FF3	135	223.7	358,082	228,090	280,000
FF4	135	195.55	419,919	287,620	344,000
FF5	160	193.7	245,690	171,650	264,000
FF6	190	330.15	141,890	95240	86000
FF7	205	322.1	114,645	80090	78000
FF8	220	267.15	99607	71640	84000
FF9	220	317.845	86647	68840	68000

Note: the fatigue crack initiation lives in the column of $N_{exp,i}$ are calculated according to the ratios of crack initiation lives to the total lives in the literature [17].

basis of their theoretical model. These percentages are different for the different cases. Because it is very difficult to obtain the crack initiation life experimentally, we adopted the result calculated according to the estimated percentage as the crack initiation life to verify our proposed approach.

In the simulation, the contact geometry between the pad and the specimen varies from cycle to cycle due to the wear. The fatigue damage value for material under the contact surface increases as the number of loading cycles increases. Therefore, the subsurface stress changes with the increasing cycle number due to the combined effects of wear and fatigue damage. Fig. 8 shows the evolution of wear scar along the contact surface for test FF9. No wear occurs at the central stick zone and wear depths at two slip zones both increase when the number of loading cycles increases from 20,000 cycles to 68,000 cycles. The deepest wear occurs at the position of $x = 0.37$ mm. Fig. 9 depicts the distribution of fatigue damage value along the contact surface after 68,000 cycles for test FF9. Fatigue damage mainly takes place in the right slip zone. The fatigue crack initiates at the position of $x = 0.37$ mm, which is in good correlation with the observed experimental results [17].

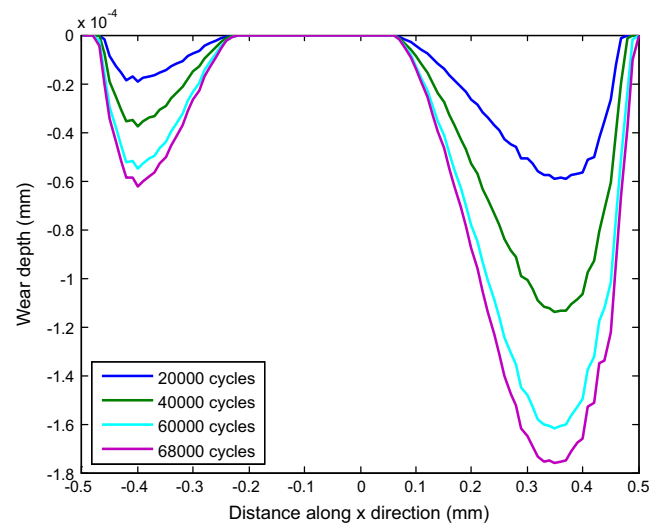


Fig. 8. Evolution of wear scar along the contact surface for test FF9.

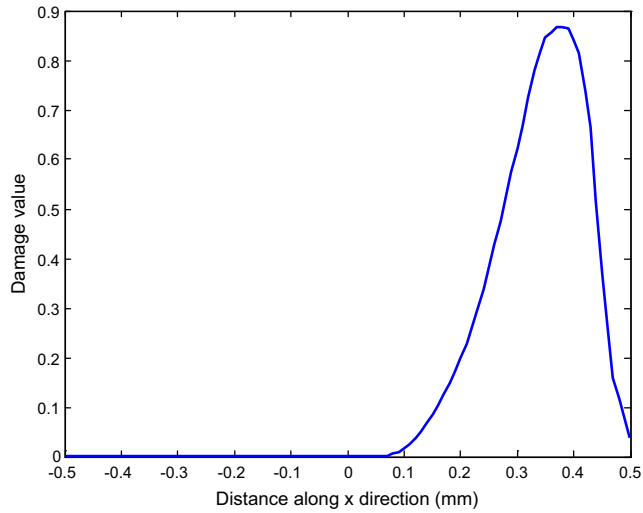


Fig. 9. Distribution of fatigue damage value along the contact surface after 68,000 cycles for test FF9.

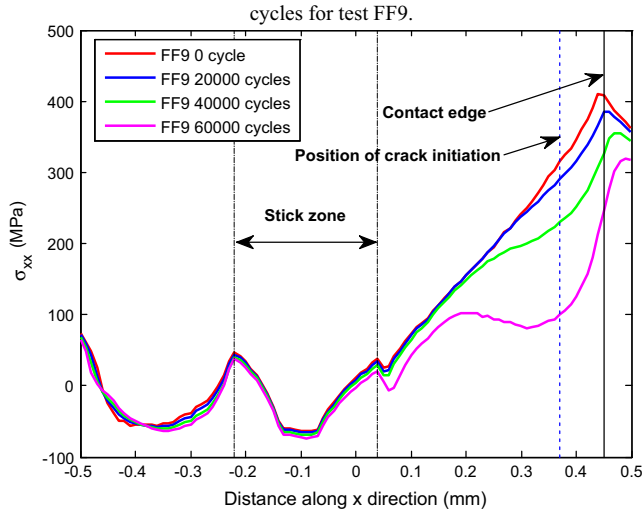


Fig. 10. Evolution of σ_{xx} along the contact surface for test FF9.

Test FF9 is continually adopted as an example to illustrate the detailed damage evolution in the specimen. The axial stress σ_{xx} of the nodes along the contact surface is a critical stress component controlling the fatigue damage, the value of which is much greater

than the contact pressure and the frictional shear stress. Fig. 10 illustrates the evolution of σ_{xx} of the nodes along the contact surface for test FF9. At the beginning of the simulation, the peak of σ_{xx} occurs at the position near the contact edge. However, due to the combined effects of wear and the non-local fatigue damage model, the stress value decreases at the damage zone and the maximum drop occurs near the position of fatigue crack initiation. Two reasons can explain this phenomenon: (1) The damage variable is coupled into the Chaboche plasticity model. The damage value at the integration point in the damage zone increases progressively as the simulation continues, which indicates the deterioration of material mechanical properties and the loss of load-carrying capacity. (2) The contact nodes in the damage zone of specimen are moved against the normal direction due to the wear, which causes a transfer of pressure to the stick zone. The detailed effects of these two factors are presented in the following subsections.

5.2. Comparison computation by four methods

In the non-local CDM approach with wear, two significant components, the non-local fatigue damage model and wear, are combined together to affect the accumulation of fatigue damage and the predicted life. The individual effect of each factor is studied in Sections 5.3 and 5.4.

In this subsection, for the purpose of comparison and investigate the effect of non-local model and wear separately, three other approaches are also employed to simulate the same cases listed in Table 2, and the results including the predicted fatigue crack initiation lives and positions are all listed in Table 3. The local fatigue damage model without considering wear is used as a baseline approach. The algorithm of which can be referred to the literature by Zhang et al. [18]. The non-local fatigue damage model without considering wear is used to reveal the effect of the non-local fatigue damage model by comparing with the baseline approach. The local fatigue damage model with considering wear is adopted as a contrastive approach to analyze the effect of wear. Fig. 11 shows the comparison between the fretting fatigue lives predicted by these four approaches and the experimental data.

5.3. Effect of non-local fatigue damage model

5.3.1. Effect on the fretting fatigue life

In order to reveal the effect of non-local fatigue damage model, the results of the first two approaches in Table 3 are compared with each other, in which the effect of wear is inexistence. Although almost all the predictions fall within the factor of two scatter bands, the local approach underestimates the crack initiation lives of eight tests except test FF5. The non-local approach gives better predictions for all nine tests than the local approach,

Table 3
Crack initiation lives and positions predicted by four approaches.

Test no.	Local CDM approach without wear		Non-local CDM approach without wear		Local CDM approach with wear		Non-local CDM approach with wear	
	$N_{pred,i}$	x/mm	$N_{pred,i}$	x/mm	$N_{pred,i}$	x/mm	$N_{pred,i}$	x/mm
FF1	520,000	0.43	690,000	0.43	540,000	0.33	650,000	0.33
FF2	324,000	0.43	416,000	0.43	388,000	0.33	464,000	0.31
FF3	190,000	0.43	232,000	0.43	250,000	0.33	280,000	0.33
FF4	226,000	0.43	280,000	0.43	292,000	0.33	344,000	0.33
FF5	174,000	0.43	212,000	0.43	234,000	0.35	264,000	0.35
FF6	67000	0.43	76000	0.41	81000	0.42	86000	0.35
FF7	61000	0.43	70000	0.41	71000	0.42	78000	0.37
FF8	65000	0.43	76000	0.41	75000	0.42	84000	0.39
FF9	55000	0.43	62000	0.39	62000	0.42	68000	0.37

Note: the FE half-width of the contact zone is 0.46 mm for all nine tests.

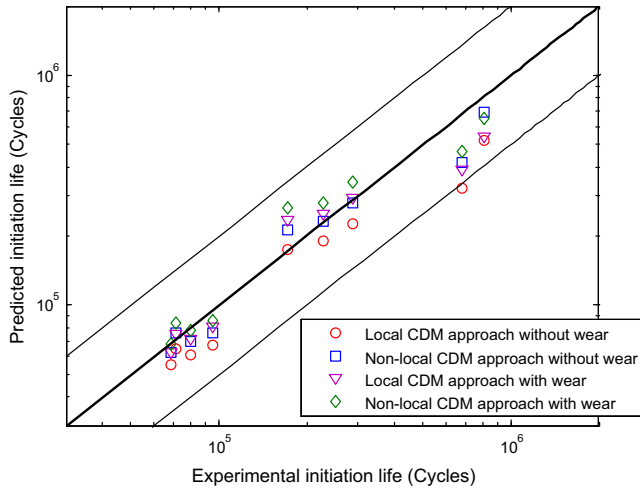


Fig. 11. Comparison between the fretting fatigue lives predicted by these three approaches and the experimental data.

which suggests the effectiveness of the non-local fatigue damage model based on DDPE. Moreover, the non-local model always brings an increase of the computational life. This is because that when the stress gradient is considered, the fatigue damage is calculated in the whole subRVE rather than just by using the maximum stress, which results in a slower damage evolution.

It is also worthy to note that the effect of non-local model has close relation with the intensity of stress gradient. Firstly, let us analyze the stresses distribution of the cases listed in Table 3. The stress concentration is obvious at the contact edge, especially for the stress component σ_{xx} . If the stress gradient and wear are both ignored, the initiation of the fretting fatigue crack occurs at the position of $x = 0.43$ mm for all nine tests. Although the configuration of the fretting fatigue experiments, such as pad radius, remains unchanged, the variation of the axial fatigue stress and tangential load can also results in the slight change of stress gradient. According to the theoretic solution of fretting contact stress in [50], the derivative of σ_{xx} near the contact edge is given by

$$\frac{d\sigma_{xx}}{dx} = p_0 \frac{x}{a^2 \sqrt{1 - (x/a)^2}} - 2\mu p_0 \frac{x - e}{ac \sqrt{((x - e)/c)^2 - 1}}, \quad e + c < x < a \quad (34)$$

where p_0 is maximum pressure, a , c and e represent semi contact width, semi sticking zone width and offset of the center of the stick zone from the center of contact zone, respectively. Since variables c and e are determined by tangential force Q and axial fatigue stress σ_{axial} , the derivative of σ_{xx} is relevant to the experimental loadings. It can be validated by comparing the distributions of normalized σ_{xx} along the contact surface at the beginning of simulation for tests FF1, FF5 and FF9, as shown in Fig. 12(a). Different trend on the increase of the stress value indicates different stress gradient as the position x approaches to the contact edge. Highest stress gradient is observed for test FF1 compared to other two tests. Besides the direction along the contact surface (x direction), the distribution of the stress component σ_{xx} in the direction of specimen width (y direction) is also needed to investigate. We choose the critical position $x = 0.43$ mm to plot the distributions of normalized σ_{xx} against the y direction for test FF1, FF5 and FF9 in Fig. 12(b). Test FF1 also have the highest stress gradient when the position y closes to the specimen surface.

Secondly, let us examine the increment of the computational life induced by non-local model. From Table 3, the ratios of the increment for test FF1, FF5 and FF9 are 32.7%, 21.8% and 12.7%

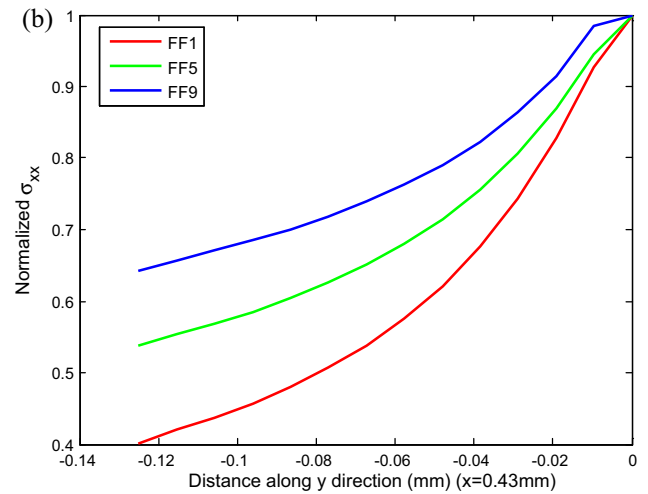
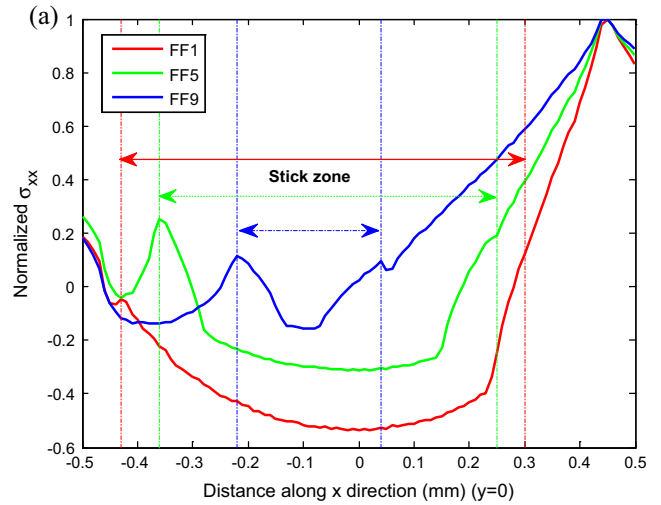


Fig. 12. Distribution of σ_{xx} along (a) x direction, (b) y direction with $x = 0.43$ mm for test FF1, FF5 and FF9.

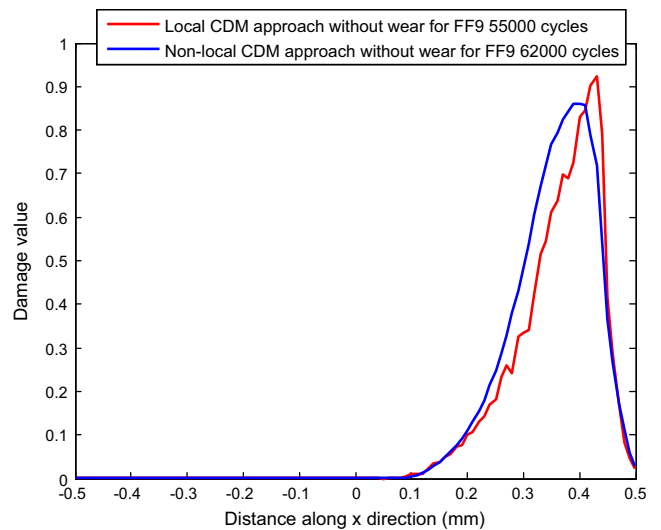


Fig. 13. Distributions of the fatigue damage along the contact surface obtained by the two approaches without wear for test FF9.

compared to the results of the local CDM approach, respectively. These results are consistent with the analysis on stress gradient in Fig. 12. Thus, it can be concluded that the effect of non-local

fatigue model on increasing the fretting fatigue life becomes more significant when the stress gradient in the subRVE is higher.

5.3.2. Effect on the position of crack initiation

The position of the fatigue crack initiation is influenced slightly by the non-local fatigue damage model, as shown in Table 3. The explanation for this point is that for these cases, although the damage evolution rate and damage distribution are changed when using non-local method, the crack initiation position determined by non-local method just locates near the critical element which is certainly the crack initiation position determined by the local method. The distributions of the fatigue damage along the contact surface obtained by the two approaches are compared for test FF9 in Fig. 13. It is noted that two distributions are plotted at the instant of fatigue crack initiation. Two peaks in the comparison figure are close to each other, both near the contact edge. But the curve predicted by the local CDM approach is much sharper than that obtained by the non-local CDM approach.

5.4. Effect of wear

5.4.1. Effect on the position of crack initiation

The direct result caused by the wear is the progressive change of the contact geometry between the pad and the specimen, which affects the distribution of the contact stress and subsurface stress. The behavior of the fretting fatigue is therefore influenced by wear.

Fig. 14 shows the distributions of wear depth along the right half contact surface at the instant of fatigue crack initiation for all nine tests. The width of the wear scar is related to the applied tangential force Q . With higher tangential force, the wear scar is wider, such as test FF6. However, the maximum depth occurs in test FF2. That is because the depth is also related to the fatigue life or the number of loading cycles, as depicted in Eq. (30). When the wear is considered, the original stress concentration position, $x = 0.43$ mm, is worn away and the position of fatigue crack initiation changes, as shown in Table 3.

5.4.2. Effect on the stress distribution

In order to clearly explain the independent effect of wear on the contact stress, it is necessary to neglect the calculation of fatigue damage, as reported in [19,26]. Additional simulations of the wear process are completed for test FF1 and FF9. The evolutions of the

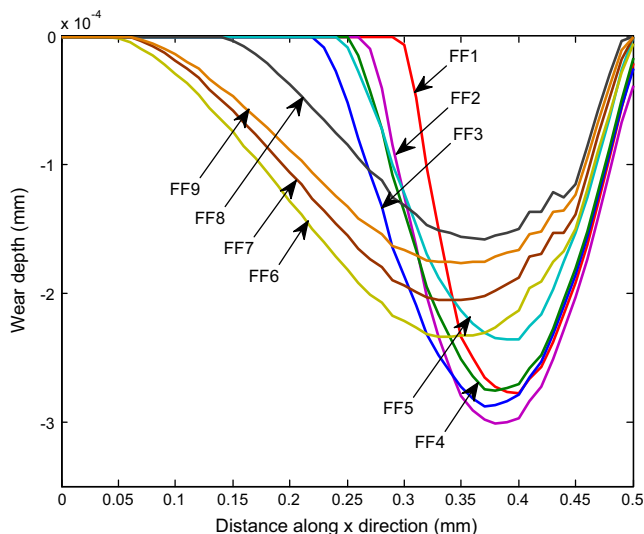


Fig. 14. Distributions of wear depth along the right half contact surface at the instant of fatigue crack initiation for all nine tests.

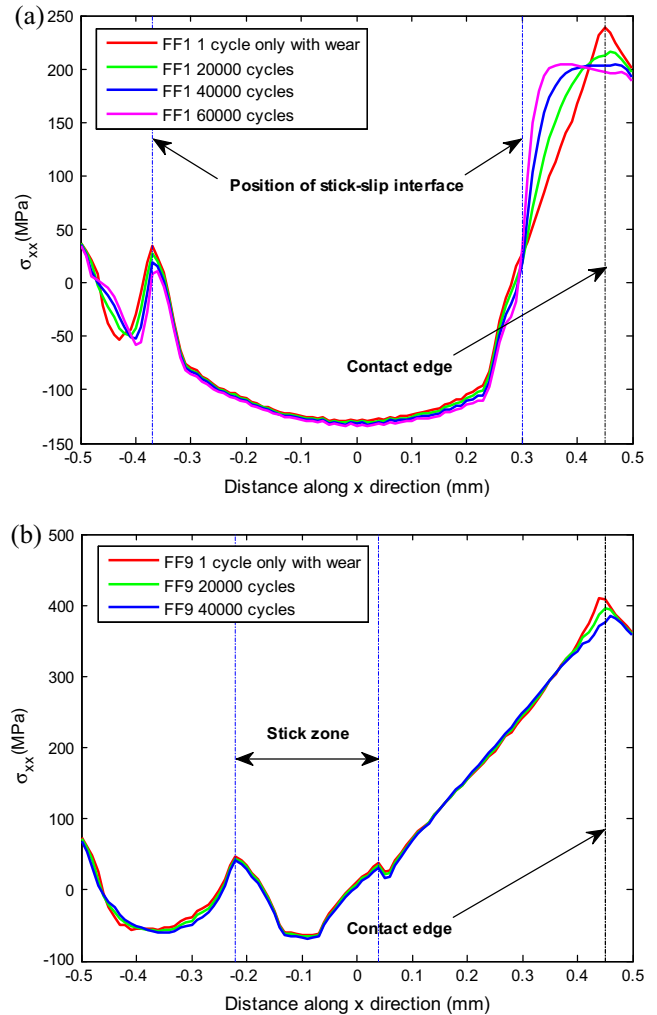


Fig. 15. Evolution of σ_{xx} along the contact surface for (a) test FF1 and (b) FF9 by considering wear only.

stress component σ_{xx} along the contact surface are illustrated for test FF1 and FF9 in Fig. 15. For test FF1, the interface between the stick zone and the slip zone is at the position of $x = 0.3$ mm. The stress value near the stick–slip interface increases as the number of fatigue cycles increases. However, the stress value at the contact edge decreases due to the movement of contact nodes. The similar results were also reported in [19,26]. Notable decline of the gradient of σ_{xx} is observed from Fig. 15(a). For test FF9, the right stick–slip interface is near the center of contact zone. The non-smooth contact geometry induced by wear is not obvious compared to the case of FF1, as shown in Fig. 14. Therefore, no significant variation of the stress value occurs near the stick–slip interface. The stress gradient also decreases due to wear, as depicted in Fig. 15(b). The conclusion can be inferred that the stress gradient near the contact edge is weakened by wear, and the maximum value of stress is decreased as well.

The effect of wear on the stress distribution finally results in the change of computational fatigue life. On the one hand, the fatigue crack initiation lives obtained by the local CDM approach with wear are higher than those predicted by the local CDM approach without wear in Table 3. That is attributed to the reduction of stress at the position of crack initiation due to wear. On the other hand, the effect of non-local fatigue model on increasing the fretting fatigue life is also diminished when considering the effect of wear. For test FF1, FF5 and FF9, the ratios of the increment on fret-

Table 4

Predicted results of fatigue lives and crack initiation positions under different wear coefficients for test FF5.

Wear coefficient, MPa ⁻¹	0	5×10^{-9}	1×10^{-8}	5×10^{-8}	1×10^{-7}
Crack initiation lives, cycles	212,000	255,000	264,000	170,000	110,000
Crack initiation position, x/mm	0.43	0.41	0.35	0.27	0.25
Positions of right stick–slip interface and right contact edge, x/mm	0.24, 0.47	0.24, 0.47	0.24, 0.47	0.23, 0.51	0.22, 0.52

ting fatigue life are 20.4%, 12.8% and 9.7% by comparing the results of the local CDM approach with wear and the non-local CDM approach with wear respectively, which are less than the ratios of increment corresponding to the two CDM approaches without wear.

5.5. Effect of wear coefficient

As the wear coefficient obtained in Section 3 doesn't match exactly with the fretting fatigue experiments modeled in this research, it is necessary to investigate the effect of wear coefficient on the fretting fatigue behavior. For local fatigue damage model in the partial slip condition, the increase of wear coefficient results in the transfer of crack initiation position from the contact edges to the stick–slip interfaces. The fretting fatigue life will increase firstly and then decrease as the wear coefficient increases [26]. In this work, we choose test FF5 as an example and conduct several simulations using non-local fatigue damage model under different wear coefficients which range from 0 to 1×10^{-7} MPa⁻¹. This range covers most of the wear coefficients for aluminum alloys. The results of fatigue lives and crack initiation positions are listed in Table 4. The positions of the right stick–slip interface and right contact edge are also listed in Table 4 for each case. The right slip zone widens slightly as the wear coefficient increases from 1×10^{-8} MPa⁻¹ to 1×10^{-7} MPa⁻¹. When the wear coefficient increases, the crack initiation position moves from near the right contact edge to near the right stick–slip interface. The effect of the wear coefficient on the fretting fatigue life is non-monotonic. The life increases slightly with the increase of wear coefficient from 0 to 1×10^{-8} MPa⁻¹, then decreases with the further increase of wear coefficient. The result shows that the wear coefficient has certain effects on the fatigue life and crack initiation position. It indicates that one should take the value of wear coefficient according to the matching experiment under the same condition as possible as one can.

6. Conclusions

A non-local fatigue damage model based on DDPE is proposed to deal with the stress gradient in fretting fatigue. By the cooperation of the damage coupled Chaboche plasticity model, a non-local CDM approach is developed and implemented in ABAQUS to predict the behavior of fretting fatigue crack initiation. The effect of wear is also considered by the utilization of the energy wear model. The predicted results are compared to the experimental data. The individual effects of the non-local fatigue damage model and wear are studied in this study. Some key findings can be concluded as follows:

- The fretting fatigue crack initiation lives predicted by the non-local CDM approach with wear agree very well with the experimental data, while the local CDM approach, whether considering wear or not, tends to underestimate the crack initiation lives compared to the experimental results.
- Four approaches all can predict applicable result for the cases studied in this paper although the result shows that the approach of the non-local model with wear is better than

others. The difference between four approaches is not significant. The reason is that the stress redistribution induced by coupled approach and contact geometry change produced by wear all reduce the effect of stress gradient. However, more significant of this study is that the effects of non-local model and wear are revealed by comparing the damage evolutions corresponding to these approaches. That will help us understand the effect of stress gradient in fretting fatigue well.

- The higher is the stress gradient in the subRVE, the more significant will be the effect of non-local fatigue model on increasing the fretting fatigue life.
- The position of the fatigue crack initiation is influenced slightly by the non-local fatigue damage model.
- The wear of the material at the contact surface relieves the loadings in the slip zone. The fatigue crack initiation lives obtained by the local CDM approach with wear are higher than those predicted by the local CDM approach without wear.
- The stress gradient near the contact edge is weakened by wear. Therefore, when considering wear, the effect of non-local fatigue model on increasing the fretting fatigue life is diminished compared with the situation when not considering wear.
- The value of wear coefficient has effects on the fatigue life and crack initiation position. Thus, one should use the wear coefficient determined by the matching experiment as possible as one can. From this point, there is a weakness in this study by adopting an estimated value due to the lack of exactly matched experimental data. We will compensate for this inadequacy in the future research.

Acknowledgment

Financial support by National Natural Science Foundation of China (11002010) is gratefully acknowledged.

References

- [1] Fouvry S, Gallien H, Berthel B. From uni- to multi-axial fretting-fatigue crack nucleation: development of a stress-gradient-dependent critical distance approach. *Int J Fatigue* 2014;62:194–209.
- [2] Araújo JA, Nowell D. The effect of rapidly varying contact stress fields on fretting fatigue. *Int J Fatigue* 2002;24:763–75.
- [3] Amargier R, Fouvry S, Chambon L, Schwob C, Poupon C. Stress gradient effect on crack initiation in fretting using a multiaxial fatigue framework. *Int J Fatigue* 2010;32:1904–12.
- [4] Szolwinski MP, Farris TN. Mechanics of fretting crack formation. *Wear* 1996;198:93–107.
- [5] Lykins CD, Mall S, Jain V. An evaluation of parameters for predicting fretting fatigue crack initiation. *Int J Fatigue* 2000;22:703–16.
- [6] Lykins CD, Mall S, Jain V. Combined experimental–numerical investigation of fretting fatigue crack initiation. *Int J Fatigue* 2001;23:703–11.
- [7] Neuber H. Theory of notch stresses: principles for exact calculation of strength with reference to structural form and material. 2nd ed. Berlin: Springer-Verlag; 1958.
- [8] Miller KJ. Materials science perspective of metal fatigue resistance. *Mater Sci Technol* 1993;9:453–62.
- [9] Naboulsi S, Mall S. Fretting fatigue crack initiation behavior using process volume approach and finite element analysis. *Tribol Int* 2003;36:121–31.
- [10] Heredia S, Fouvry S, Berthel B, Greco E. Introduction of a principal stress–weight function approach to predict the crack nucleation risk under fretting fatigue using FEM modelling. *Int J Fatigue* 2014;61:191–201.
- [11] Lemaitre J, Rodrigue D. Engineering damage mechanics. Berlin: Springer; 2005.
- [12] Marmi AK, Habraken AM, Duchene L. Multiaxial fatigue damage modelling at macro scale of Ti–6Al–4V alloy. *Int J Fatigue* 2009;31:2031–40.

- [13] Lemaitre J, Chaboche JL. *Mechanics of solid materials*. New ed. Cambridge: Cambridge University Press; 1994.
- [14] Papadopoulos IV. Invariant formulation of gradient dependent multiaxial high cycle fatigue criterion. *Eng Fract Mech* 1996;55(4):513–28.
- [15] Hojjati-Talemi R, Wahab MA. Fretting fatigue crack initiation lifetime predictor: using damage mechanics approach. *Tribol Int* 2013;60:176–86.
- [16] Hojjati-Talemi R, Wahab MA, Giner E, Sabsabi M. Numerical estimation of fretting fatigue lifetime: using damage and fracture mechanics. *Tribol Lett* 2013;52:11–25.
- [17] Hojjati-Talemi R, Wahab MA, De Pauw J, De Baets P. Prediction of fretting fatigue crack initiation and propagation lifetime for cylindrical contact configuration. *Tribol Int* 2014;76:73–91.
- [18] Zhang T, McHugh PE, Leen SB. Finite element implementation of multiaxial continuum damage mechanics for plain and fretting fatigue. *Int J Fatigue* 2012;44:260–72.
- [19] Shen F, Hu WP, Meng QC. A damage mechanics approach to fretting fatigue life prediction with consideration of elastic–plastic damage model and wear. *Tribol Int* 2015;82:176–90.
- [20] Walvekar AA, Leonard BD, Sadeghi F, Jalalahmadi B, Bolander N. An experimental study and fatigue damage model for fretting fatigue. *Tribol Int* 2014;79:183–96.
- [21] McColl IR, Ding J, Leen SB. Finite element simulation and experimental validation of fretting wear. *Wear* 2004;256:1114–27.
- [22] Madge JJ, Leen SB, Shipway PH. The critical role of fretting wear in the analysis of fretting fatigue. *Wear* 2007;263:542–51.
- [23] Madge JJ, Leen SB, McColl IR, Shipway PH. Contact-evolution based prediction of fretting fatigue life: effect of slip amplitude. *Wear* 2007;262:1159–70.
- [24] Zhang T, McHugh PE, Leen SB. Computational study on the effect of contact geometry on fretting behavior. *Wear* 2011;271:1462–80.
- [25] Jin O, Mall S. Effects of independent pad displacement on fretting fatigue behavior of Ti–6Al–4V. *Wear* 2002;253:585–96.
- [26] Shen F, Hu WP, Voyiadjis GZ, Meng QC. Effects of fatigue damage and wear on fretting fatigue under partial slip condition. *Wear* 2015;338–339:394–405.
- [27] Murakami S. *Continuum damage mechanics*. New York: Springer; 2012.
- [28] McDowell DL, Dunne FPE. Microstructure-sensitive computational modeling of fatigue crack formation. *Int J Fatigue* 2010;32:1521–42.
- [29] Castelluccio GM, Musinski WD, McDowell DL. Recent developments in assessing microstructure sensitive early stage fatigue of polycrystals. *Curr Opin Solid St Mater* 2014;18:180–7.
- [30] Voyiadjis GZ, Kattan PI. A comparative study of damage variables in continuum damage mechanics. *Int J Damage Mech* 2009;18:315–40.
- [31] Voyiadjis GZ, Kattan PI. Mechanics of damage processes in series and in parallel: a conceptual framework. *Acta Mech* 2012;223:1863–78.
- [32] Chaboche JL. Constitutive equations for cyclic plasticity and cyclic viscoplasticity. *Int J Plast* 1989;5:247–302.
- [33] Zhang M, Neu RW, McDowell DL. Microstructure-sensitive modeling: application to fretting contacts. *Int J Fatigue* 2009;31:1397–406.
- [34] McCarthy OJ, McGarry JP, Leen SB. Microstructure-sensitive prediction and experimental validation of fretting fatigue. *Wear* 2013;305:100–14.
- [35] Ghosh S, Chakraborty P. Microstructure and load sensitive fatigue crack nucleation in Ti-6242 using accelerated crystal plasticity FEM simulations. *Int J Fatigue* 2013;48:231–46.
- [36] Lemaitre J. *A course on damage mechanics*. Berlin: Springer-Verlag; 1992.
- [37] Xiao YC, Li S, Gao Z. A continuum damage mechanics model for high cycle fatigue. *Int J Fatigue* 1998;20:503–8.
- [38] Chaudonneret M. Simple efficient multiaxial fatigue damage model for engineering applications macro crack initiation. *J Eng Mater Technol* 1993;115(4):373–9.
- [39] Sines G. *Behavior of metals under complex static and alternating stresses*. Metal fatigue, New York: McGraw Hill; 1959, p. 145–69.
- [40] Azari Z, Abbadi M, Moustabchir H, Lebienvenu M. The influence of fatigue cycling on the oxidation kinetics and crack initiation of a Cr–Mo steel. *Int J Fatigue* 2008;30:517–27.
- [41] Nasr A, Nadot Y, Bouraoui C, Fathallah R, Jouiad M. Fatigue initiation in C35 steel: influence of loading and defect. *Int J Fatigue* 2010;32:780–7.
- [42] Musinski WD, McDowell DL. Microstructure-sensitive probabilistic modeling of HCF crack initiation and early crack growth in Ni-base superalloy IN100 notched components. *Int J Fatigue* 2012;37:41–53.
- [43] *Metallic Materials and Elements for Aerospace Vehicle Structures*. Military Handbook MIL-HDBK-5H. U.S. Department of Defense; 1998.
- [44] Szolwinski MP, Farris TN. Observation, analysis and prediction of fretting fatigue in 2024-T351 aluminum alloy. *Wear* 1998;221:24–36.
- [45] Magaziner RS, Jain VK, Mall S. Wear characterization of Ti–6Al–4V under fretting-reciprocating sliding conditions. *Wear* 2008;264:1002–14.
- [46] Antunes PV, Ramalho A. Fretting behaviour of glass-fibre-reinforced polypropylene composite against 2024 Al alloy. *Tribol Int* 2005;38:363–79.
- [47] Huda Z, Taib NI, Zaharinie T. Characterization of 2024-T3: an aerospace aluminum alloy. *Mater Chem Phys* 2009;113:515–7.
- [48] Merati A. A study of nucleation and fatigue behavior of an aerospace aluminum alloy 2024-T3. *Int J Fatigue* 2005;27:33–44.
- [49] ABAQUS/Standard Version 6.10, User Manual. Hibbit Karlsson and Sorensen Inc, Rhode Island, USA; 2010.
- [50] Hills DA, Nowell D. *Mechanics of fretting fatigue*. Dordrecht: Kluwer Academic; 1994.